The polarization of bremsstrahlung from radiative ionization induced by relativistic highly charged projectiles

D H Jakubaßa-Amundsen

Mathematics Institute, University of Munich, Theresienstrasse 39, 80333 Munich, Germany

Abstract
Based on inverse kinematics the close relation between radiative electron capture to the projectile continuum, calculated within the impulse approximation, and electron–nucleus bremsstrahlung is shown. Particular emphasis is laid on the short-wavelength limit corresponding to cusp-electron emission in the target frame of reference. Differential cross sections and the degree of photon polarization are calculated for the coincident emission of electron and photon. Coplanar and non-coplanar geometries are considered, and the polarization is compared with that obtained from experiments on the elementary bremsstrahlung process and on radiative electron capture to bound states.

1. Introduction

The interest in radiation phenomena during heavy ion–atom collisions has been revived by the feasibility of experiments where fast forward electrons are recorded in coincidence with the emitted photons. Pioneer measurements of the cusp-electron spectrum and the accompanying photon spectra for 90 MeV amu^{-1} U^{88+} + N$_2$ collisions were carried out at the GSI Darmstadt, Germany [1, 2]. The collision velocity was in a regime where the radiation process is still strongly dominated by the nonradiative Coulomb capture to continuum [3]. Therefore, a coincidence experiment is mandatory to single out the electrons related to radiation.

An important reason for studying the radiative capture of a loosely bound target electron into a continuum projectile eigenstate close to threshold (the radiative ionization (RI) [4] sometimes also termed RECC) is its relation—by inverse kinematics—to the short-wavelength limit (SWL) of the elementary process of electron–nucleus bremsstrahlung. Since in the SWL the electron is slowed down to near-zero energy and is thus hard to detect, the fact that it appears as a cusp electron in the target frame of reference opens the possibility for an experimental investigation of the SWL for bremsstrahlung on highly charged ions.

There exists a vast literature on the theory of bremsstrahlung which can be profited of once the relation to RI is established. Early work dates back to Bethe and Heitler [5] using

the Born approximation, and to Bess [6], Maximon and Bethe [7] apply Sommerfeld–Maue wavefunctions for the electron. These functions got established in bremsstrahlung calculations by the seminal work of Elwert and Haug [8], and their applicability for the differential cross sections was supported by later calculations using exact relativistic wavefunctions [9–12]. An overview of the calculations in comparison with experimental data (far off the SWL) can be found in [13–16].

A second process related to RI by means of continuity across the ionization threshold [17] is the radiative electron capture (REC) into bound states of heavy projectiles. Viewed as inverse photoeffect, the REC has attracted much interest during the recent years both theoretically and experimentally [18]. In particular, the impulse approximation combined with exact relativistic wavefunctions [19] has proved to give an excellent description of the experimental photon momentum distributions [20, 21].

The aim of the present work is, apart from studying cusp features, the investigation of the angular distribution and linear polarization of the RI photons in the context of their relation to bremsstrahlung and REC. Thereby future experiments should be stimulated which combine the use of a Compton polarimeter [22] with the electron–photon coincidence detection technique [1, 2].

As concerns the polarization studies we restrict ourselves to the photon linear polarization, the only one which is accessible if electron polarization is disregarded [23]. There is some early theoretical work on the photoeffect by polarized photons (see, e.g., [24]), and recently also the REC photon polarization was calculated for a few cases [25, 26]. The bremsstrahlung polarization, on the other hand, has been thoroughly investigated (see, e.g., [27–30]). However, most of these studies involve doubly differential cross sections (where the electron angular distribution is integrated over). The polarization from the elementary bremsstrahlung process (concerning *triply* differential cross sections) is much different [31] which was confirmed by experiment [31, 32]. Since in the nonrelativistic limit (for coplanar geometry) the bremsstrahlung photons are completely polarized in the plane spanned by the incoming electron and the emitted photon [28], any depolarization points to the importance of the relativistic dynamics or spin-flip effects [29].

The paper is organized as follows. In section 2, the relativistic RI theory is outlined and some (target-frame) results on the photon angular distribution for forward emitted electrons are given. The bremsstrahlung limit of RI is derived in section 3 and its approach with decreasing target nuclear charge is investigated numerically. Section 4 is devoted to structures in the projectile-frame differential cross section and to spin-flip effects. The cusp asymmetry and its dependence on the photon emission angle is studied in section 5. In section 6, the photon linear polarization and its dependence on the electron and photon momenta, on the collision velocity as well as on the projectile and target nuclear charge, is investigated for the coplanar geometry. Section 7 presents the results for the non-coplanar geometry and a comparison with the experimental polarization of bremsstrahlung photons [31]. The relation between RI and REC and the polarization results for the two processes in the case of bare uranium projectiles are discussed in section 8. Concluding remarks are made in section 9. Atomic units ($\hbar = m = e = 1$) are used unless otherwise indicated.

2. Radiative ionization in the laboratory frame

The relativistic formulation of radiative ionization in the impulse approximation (IA) is given in a previous work [33]. Briefly, the four-fold differential cross section for the simultaneous emission of a target electron with energy E_f (and momentum k_f) into the solid angle $\mathrm{d}\Omega_f$

and a photon with energy $\omega = kc$ and polarization direction e_λ into the solid angle $d\Omega_k$ is (in the target frame of reference) given by

$$\frac{d^4\sigma_\lambda}{dE_f\, d\Omega_f\, d\omega\, d\Omega_k} = \frac{k_f \omega \omega' E'_f}{2c^5} \sum_{\sigma_i,\sigma_f} \int d^2b \left|a^{IA}_{fi,\lambda}\right|^2 \tag{2.1}$$

where the projectile is assumed to move along a straight-line path with impact parameter b. Since the initial electron is unpolarized and the polarization of the ejected electron is not observed, we have averaged over the initial spin states (σ_i) and summed over the final ones (σ_f). For the transition amplitude we have

$$a^{IA}_{fi,\lambda} = \frac{2\pi i}{\gamma} \sqrt{\frac{1+\gamma}{2}} A'_\lambda \sum_{s=1}^{4} \int dq\, e^{iq_\perp b} W_{rad}(\sigma_f, s, q)$$
$$\times \left[u^{(s)+}_q \left(1 - \frac{\gamma v/c}{1+\gamma}\alpha_z\right) \varphi^{(\sigma_i)}_{i,T}(p) \right] \delta\left(E'_f + \omega' - E^T_i/\gamma + q_z v\right) \tag{2.2}$$

with the photon field $A'_\lambda = c e_\lambda / (2\pi \omega'^{\frac{1}{2}})$ and a relativistic 4-spinor $u^{(s)}_q$ (defined in the appendix) characterized by momentum q and spin $s(s = 1, 2$ for the particle states and $s = 3, 4$ for the antiparticle states)[1]. The initial-state wavefunction in momentum space is denoted by $\varphi^{(\sigma_i)}_{i,T}(p)$ with $p = (q_\perp, E^T_i v/c^2 + q_z/\gamma)$ in cylindrical coordinates, E^T_i being the initial-state energy of the electron. The radiation matrix element between the intermediate ($\psi^{(s)}_{q,P}$) and the final ($\psi^{(\sigma_f)}_{f,P}$) projectile scattering eigenstates is given by

$$W_{rad}(\sigma_f, s, q) = \int dx'\, \psi^{(\sigma_f)+'}_{f,P}(x') \alpha\, e^{-ik'x'} \psi^{(s)'}_{q,P}(x') \tag{2.3}$$

with the Dirac matrices $\alpha = (\alpha_x, \alpha_y, \alpha_z)$ and k the photon momentum. Primed quantities refer to the projectile reference frame, and the momentum 4-vectors are interrelated by a Lorentz transformation, namely

$$E'_f = \gamma(E_f - v k_f \cos\vartheta_f), \qquad \omega' = \gamma\omega\left(1 - \frac{v}{c}\cos\vartheta_k\right)$$
$$\cos\vartheta'_f = \frac{\gamma}{k'_f}\left(-\frac{vE_f}{c^2} + k_f\cos\vartheta_f\right), \qquad \cos\vartheta'_k = \frac{\cos\vartheta_k - \frac{v}{c}}{1 - \frac{v}{c}\cos\vartheta_k} \tag{2.4}$$

with $\gamma = (1 - v^2/c^2)^{-1/2}$. Note that the inverse transformation is obtained upon replacing v by $-v$ throughout. The collision velocity $v = v e_z$ is taken in the z-direction and the x-axis is defined such that the photon momentum lies in the (x, z)-plane, $k' = k'(\sin\vartheta'_k, 0, \cos\vartheta'_k)$. Then, the two photon polarization directions, perpendicular to k', are taken as

$$e_{\lambda_1} = (0, 1, 0), \qquad e_{\lambda_2} = (-\cos\vartheta'_k, 0, \sin\vartheta'_k). \tag{2.5}$$

We will refer to e_{λ_2} as 'in-plane' linear polarization and e_{λ_1} as 'perpendicular' polarization.

Following [34] we define the degree of the photon linear polarization by

$$P = \frac{d\sigma_{\lambda_2} - d\sigma_{\lambda_1}}{d\sigma_{\lambda_2} + d\sigma_{\lambda_1}} \tag{2.6}$$

where $d\sigma_{\lambda_i}$ abbreviates the (multiply) differential cross section corresponding to the polarization direction e_{λ_i}, $i = 1, 2$. The denominator, $d\sigma_{\lambda_1} + d\sigma_{\lambda_2} \equiv d\sigma$, is the differential RI cross section if the photon polarization is not observed. The definition (2.6) of P coincides with the Stokes parameter C_{03} [23]. In the bremsstrahlung literature, P is usually defined with a negative sign (see, e.g., [27, 30]).

---

[1] In previous work [3, 33] this spin sum was erroneously truncated at $s = 2$. However, the contribution of $s = 3, 4$ in the weakly relativistic regime considered is negligibly small.
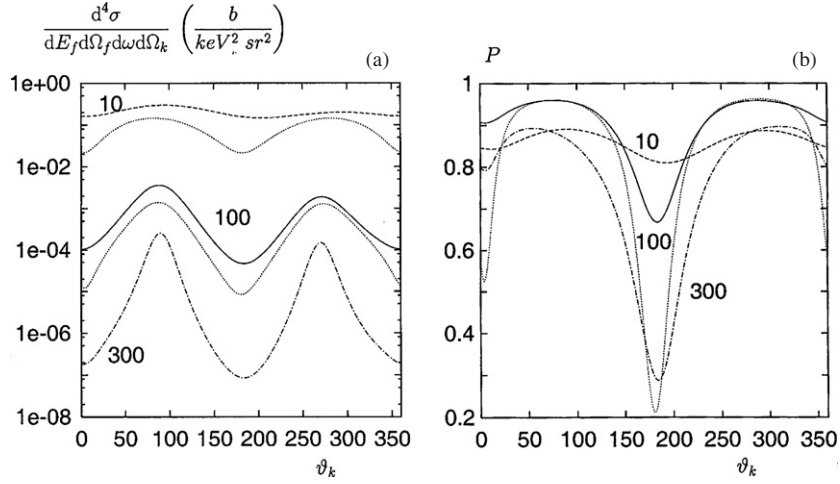
Figure 1. Four-fold differential cross section (a) and polarization (b) for K-shell RI from Ag^{47+}+Ar as a function of ϑ_k. Long-broken curve, full curve and chain curve correspond to cusp electrons with kinetic energy $E_{f,kin} = \tilde{E}_0 = 10$, 100 and 300 keV, respectively, emitted at $\vartheta_f = 1°$, $\varphi = 0$. Dotted curves in (a) $E_{f,kin} = 12$, $\tilde{E}_0 = 10$ (upper curve) and $E_{f,kin} = 110$, $\tilde{E}_0 = 100$ (lower curve). Dotted curve in (b) $E_{f,kin} = 110$, $\tilde{E}_0 = 100$. Photon energy $\omega = \omega_{peak}(90°)$ from (2.7): $\omega = 5.4$ for $E_{f,kin} = \tilde{E}_0 = 10$; 5.31 for $E_{f,kin} = 12$, $\tilde{E}_0 = 10$; 79.2 for $E_{f,kin} = \tilde{E}_0 = 100$; 79.0 for $E_{f,kin} = 110$, $\tilde{E}_0 = 100$; 184.5 for $E_{f,kin} = \tilde{E}_0 = 300$ (all energies in keV).

Figure 1(a) shows the differential RI cross section (summed over λ) for bare Ag impinging on a hydrogenic (one-electron) Ar target as a function of the photon emission angle. The collision velocity, or equivalently the kinetic energy of a free target electron in the projectile reference frame, $\tilde{E}_0 \equiv E'_0 - mc^2 = (\gamma - 1)mc^2$, is treated as parameter. Then $v = 26.72$, 75.13, 106.42 au correspond, respectively, to $\tilde{E}_0 = 10$, 100, 300 keV. The photon frequency is kept fixed, and the electron (which is either a cusp electron, $E'_f \approx mc^2$, or has a kinetic energy of a few keV) is ejected into the forward direction. The coplanar geometry is chosen where the electron is emitted into the (x, z)-plane (i.e. electron, photon and the beam axis lie in one plane). Then $0° < \vartheta_k < 180°$ (and $\varphi \equiv \varphi_f - \varphi_k = 0$ where φ_f and φ_k denote the azimuthal angles of electron and photon, respectively) means emission of both particles into the same hemisphere, while $180° < \vartheta_k < 360°$ and $\varphi = 0$ (or, respectively, $180° > \vartheta_k > 0°$ and $\varphi = 180°$) refer to the case where electron and photon are emitted into opposite sides of the beam axis. There is a rather strong left–right asymmetry, although ϑ_f is very small (but $\neq 0$).

Moreover, as expected, the cross section decreases with velocity and the peak near $\vartheta_k = 90°$ gets narrower. To understand the second item, we recall that the differential RI cross section (2.1) with (2.2) is basically proportional to the Compton profile of the target electron. For spherically symmetric initial states the energy-conserving delta function (together with the requirement $p = 0$ for the peak maximum) leads to the condition $\omega' = E_i^T/\gamma - q_z v - E'_f$ with $q_z/\gamma = -E_i^T v/c^2$. For fixed E'_f, this translates to the peak condition for the photon energy (in the projectile and target frame, respectively, cf (2.4))

$$\omega' = \gamma E_i^T - E'_f \equiv \omega'_{peak}, \qquad \omega = \frac{\gamma E_i^T - E'_f}{\gamma\left(1 - \frac{v}{c}\cos\vartheta_k\right)} \equiv \omega_{peak}(\vartheta_k). \qquad (2.7)$$

Whereas nonrelativistically ($v/c \to 0$, $\gamma \to 1$)ω_{peak} is a constant, (2.7) shows its dependence on the photon emission direction. One has $\omega_{peak}(0) = \gamma^2 \omega_{peak}(90°)\left(1 + \frac{v}{c}\right)$ and, therefore,
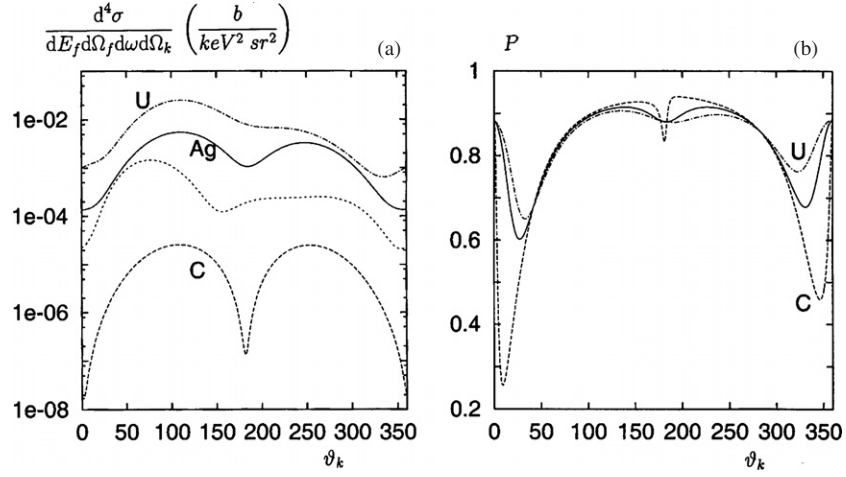
Figure 2. Four-fold differential cross section (a) and polarization (b) for RI from P + H at $\bar{E}_0 = 300$ keV as a function of ϑ_k. P = C^{6+} (— — —), Ag^{47+} (———), U^{92+}(— · — · —·). Spin-flip contribution for uranium (- - - - -). The parameters are $E_{f,kin} = 300$ keV, $\vartheta_f = 1°$, $\varphi = 0$ and $\omega = \omega_{peak}(\vartheta_k)$.

$\omega_{peak}(0) - \omega_{peak}(90°) \sim v\gamma^2$. This has to be compared with the width of the Compton profile which behaves like $\omega - \omega_{peak}(90°) \sim v$ [33] and thus increases much slower with v. If at $\vartheta_k = 0$ the RI cross section is calculated with $\omega = \omega_{peak}(90°)$, it sits on the wing of the Compton profile (the farther away from the maximum the higher the v).

Figure 2(a) shows the differential RI cross section for a series of bare projectiles colliding with H as a function of ϑ_k. Probed is again the cusp region, but now at each ϑ_k, ω is chosen according to (2.7). This corresponds to the experimental situation where all photons are recorded which are emitted into a fixed direction (the main contribution coming from those with $\omega \approx \omega_{peak}(\vartheta_k)$). The cross section maximum has shifted to a slightly higher angle as compared to the case of the fixed ω, and there is hardly any decrease of the peak width with v. An increase of the projectile charge leads only to a slight increase of the width, but to considerably larger cross sections.

3. The bremsstrahlung limit of RI

When the target potential decreases to zero the electron becomes free. Viewed from the projectile frame of reference, this electron scatters with velocity $-v$ inelastically from the projectile, emitting a photon. In this section, we give a derivation of the bremsstrahlung limit.

To start with, the differential RI cross section (2.1) is transformed into the projectile frame of reference by using the fact that the phase space element $c^2 \, d\mathbf{k}/E$ is a relativistic invariant [35, p 124],

$$\frac{d^4\sigma'_\lambda}{dE'_f \, d\Omega'_f \, d\omega' \, d\Omega'_k} = \frac{\omega' k'_f}{\omega k_f} \frac{d^4\sigma_\lambda}{dE_f \, d\Omega_f \, d\omega \, d\Omega_k}$$
$$= \frac{\omega'^2 k'_f E'_f}{2c^5} \sum_{\sigma_i,\sigma_f} \int d^2\mathbf{b} \left| a^{IA}_{fi,\lambda} \right|^2 , \tag{3.1}$$

with $a^{IA}_{fi,\lambda}$ from (2.2).

In the bremsstrahlung case we know from energy conservation that $E'_f = E'_0 - \omega'$ is fixed if ω' is fixed. In order to derive the bremsstrahlung limit from (3.1) we therefore have to integrate over E'_f, keeping in mind that the target function $\varphi_{i,T}^{(\sigma_i)}(\boldsymbol{p})$ becomes proportional to $\delta(\boldsymbol{p})$ for $Z_T \to 0$.

When Z_T approaches 0 the relativistic bound-state function turns into a Darwin function [36] (which is exact up to first order in Z_T/c and which is used in our calculations throughout). For an $l_i = 0$ state its momentum representation reads

$$\varphi_{i,T}^{(\sigma_i)}(\boldsymbol{p}) = N_i^T a_i^{(\sigma_i)}(\boldsymbol{p})\tilde{\varphi}_{i,T}(\boldsymbol{p})$$

$$N_i^T = \left[1 + \left(\frac{Z_T\mu}{n_i}\right)^2\right]^{-\frac{1}{2}}, \qquad a_i^{(1)}(\boldsymbol{p}) = \begin{pmatrix} 1 \\ 0 \\ \mu p_z \\ \mu p_+ \end{pmatrix}, \qquad a_i^{(2)}(\boldsymbol{p}) = \begin{pmatrix} 0 \\ 1 \\ \mu p_- \\ -\mu p_z \end{pmatrix} \tag{3.2}$$

with $p_\pm = p_x \pm i p_y$, $\mu = c/(E_i^T + c^2)$ and $\tilde{\varphi}_{i,T}(\boldsymbol{p})$ the nonrelativistic bound-state momentum-space wavefunction (with quantum numbers $n_i, l_i = 0, m_i = 0$).

Introducing $F_{\boldsymbol{q}}(E'_f, \omega')$ by means of

$$a_{fi,\lambda}^{\mathrm{IA}} \equiv \int \mathrm{d}\boldsymbol{q}\, \mathrm{e}^{\mathrm{i}\boldsymbol{q}_\perp \boldsymbol{b}} F_{\boldsymbol{q}}(E'_f, \omega')\varphi_{i,T}^{(\sigma_i)}(\boldsymbol{p})\delta\left(E'_f + \omega' - E_i^T/\gamma + q_z v\right), \tag{3.3}$$

we obtain

$$Q_\lambda(\omega') \equiv \int_{c^2}^{\infty} \mathrm{d}E'_f\, k'_f E'_f \int \mathrm{d}^2\boldsymbol{b}\, \left|a_{fi,\lambda}^{\mathrm{IA}}\right|^2$$
$$= \frac{(2\pi)^2}{v^2}\left(N_i^T\right)^2 \int_{c^2}^{\infty} \mathrm{d}E'_f\, k'_f E'_f \int \mathrm{d}\boldsymbol{q}_\perp \left|F_{\boldsymbol{q}}(E'_f, \omega')a_i^{(\sigma_i)}(\boldsymbol{p})\tilde{\varphi}_{i,T}(\boldsymbol{p})\right|^2 \tag{3.4}$$

with $q_z = -\frac{1}{v}\left(E'_f + \omega' - E_i^T/\gamma\right)$. From the definition of p_z, we can substitute p_z for E'_f by means of

$$E'_f = -p_z\gamma v - \omega' + \gamma E_i^T \tag{3.5}$$

such that $\int_{c^2}^{\infty} \mathrm{d}E'_f = \gamma v \int_{-\infty}^{p_1} \mathrm{d}p_z$ with $p_1 = \left(-c^2 - \omega' + \gamma E_i^T\right)/\gamma v$. We note that $p_1 = 0$ if $\omega' = \gamma E_i^T - c^2$ which is the largest possible photon energy if the width of the initial-state momentum distribution is neglected, and $p_1 > 0$ for smaller ω'.

Let us restrict ourselves to the target 1s state. Then for small Z_T, $\tilde{\varphi}_{i,T}(\boldsymbol{p})$ is strongly peaked at $p = 0$ where q_z takes the value $q_z(0) = -\gamma E_i^T v/c^2 \neq 0$. Thus for sufficiently small Z_T, the function $F_{\boldsymbol{q}}(E'_f, \omega')a_i^{(\sigma_i)}(\boldsymbol{p})$ is continuous in $\boldsymbol{p}$ and therefore can be taken outside the integral at $p = 0$ (this peaking approximation becomes exact in the limit $Z_T \to 0$). Using the definition of $F_{\boldsymbol{q}}(E'_f, \omega')$ by identification of (3.3) with (2.2) this results in

$$Q_\lambda(\omega') \approx \frac{(2\pi)^2\gamma}{v}\left(N_i^T\right)^2 k'_f E'_f \left|F_{q_z(0)\boldsymbol{e}_z}(E'_f, \omega')u_0^{(\sigma_i)}\right|^2 \int_{-\infty}^{p_1} \mathrm{d}p_z \int \mathrm{d}\boldsymbol{q}_\perp |\tilde{\varphi}_{i,T}(\boldsymbol{q}_\perp, p_z)|^2,$$

$$F_{q_z(0)\boldsymbol{e}_z}(E'_f, \omega') = \frac{2\pi\mathrm{i}}{\gamma}\sqrt{\frac{1+\gamma}{2}}\boldsymbol{A}'_\lambda \sum_{s=1}^{4} \boldsymbol{W}_{\mathrm{rad}}(\sigma_f, s, q_z(0)\boldsymbol{e}_z)u_{q_z(0)\boldsymbol{e}_z}^{(s)+}\left(1 - \frac{\gamma v/c}{1+\gamma}\alpha_z\right), \tag{3.6}$$

with E'_f from (3.5) for $p_z = 0$. We have used $a_i^{(\sigma_i)}(0) = u_0^{(\sigma_i)} = (1, 0, 0, 0)^+$ for $\sigma_i = 1$ and $(0, 1, 0, 0)^+$ for $\sigma_i = 2$.

Recalling that $\int \mathrm{d}\boldsymbol{q}_\perp |\tilde{\varphi}_{i,T}(\boldsymbol{q}_\perp, p_z)|^2$ is equal to the Compton profile, $\tilde{J}_i(p_z) = \frac{8Z_T^5}{3\pi}\left[Z_T^2 + p_z^2\right]^{-3}$ (for a 1s state), the integral in (3.6) gives $\frac{1}{2}$ for $p_1 = 0$. For $p_1 > 0$ on the other hand, it approaches 1 in the limit $Z_T \rightarrow 0$. For the prefactor in (3.6) we have the identity (cf (A.2))

$$\sqrt{\frac{1+\gamma}{2\gamma}}\left(1 - \frac{\gamma v/c}{1+\gamma}\alpha_z\right)u_0^{(\sigma_i)} = u_{-\gamma v}^{(\sigma_i)}. \tag{3.7}$$

Thus, the bremsstrahlung limit reads for $\omega' < (\gamma - 1)c^2$, using the orthogonality of the 4-spinors, $u_{-\gamma v}^{(s)+}u_{-\gamma v}^{(\sigma_i)} = \delta_{s,\sigma_i}$,

$$\frac{\mathrm{d}^3\sigma_\lambda^{\prime\mathrm{brems}}}{\mathrm{d}\Omega'_f\,\mathrm{d}\omega'\,\mathrm{d}\Omega'_k} = \lim_{Z_T \rightarrow 0}\frac{\mathrm{d}^3\sigma'_\lambda}{\mathrm{d}\Omega'_f\,\mathrm{d}\omega'\,\mathrm{d}\Omega'_k} = \lim_{Z_T \rightarrow 0}\frac{\omega'^2}{2c^5}\sum_{\sigma_i,\sigma_f}Q_\lambda(\omega')$$

$$= \frac{8\pi^4\omega'^2 k'_f E'_f}{c^5 v}\sum_{\sigma_i,\sigma_f}|\boldsymbol{A}'_\lambda \boldsymbol{W}_{\mathrm{rad}}(\sigma_f, \sigma_i, -\gamma v)|^2 \tag{3.8}$$

where (3.5) now turns into $E'_f = \gamma c^2 - \omega'$. (One has to keep in mind that at the SWL, $\omega' = (\gamma - 1)c^2$, the rhs of (3.8) is smaller by a factor of 2.)

When Sommerfeld–Maue functions are used (which is done throughout in the present work) one gets a closed expression for the radiation matrix element [7, 8]. Then, the bremsstrahlung limit reduces to

$$\frac{\mathrm{d}^3\sigma_\lambda^{\prime\mathrm{brems}}}{\mathrm{d}\Omega'_f\,\mathrm{d}\omega'\,\mathrm{d}\Omega'_k} = \frac{\omega' k'_f E'_f}{8\pi^2 c^3 v}\frac{\eta_q}{1 - e^{-2\pi\eta_q}}\frac{\eta_f}{1 - e^{-2\pi\eta_f}}\sum_{\sigma_i,\sigma_f}\left|\left(u_{k'_f}^{(\sigma_f)+}(\boldsymbol{e}_\lambda \boldsymbol{I})u_q^{(\sigma_i)}\right)\right|^2 \tag{3.9}$$

with $\boldsymbol{q} = -\gamma v$, $\eta_q = Z_P E_q/qc^2$ and $\eta_f = Z_P E'_f/k'_f c^2$ the Sommerfeld parameters (where $E_q = (q^2 c^2 + c^4)^{\frac{1}{2}}$) and $\boldsymbol{I}$ an analytic expression (see the appendix). (3.9) is identical to the Elwert–Haug bremsstrahlung formula [8].

Rather than to reverse the beam direction in the comparison of RI with the bremsstrahlung results it is more convenient to redefine the emission angles. We define the projectile-frame emission angles θ'_f and θ'_k by

$$\theta'_f = \pi - \vartheta'_f, \qquad \theta'_k = \pi - \vartheta'_k \tag{3.10}$$

where ϑ'_f and ϑ'_k are the Lorentz-transformed target-frame emission angles.

In figure 3(a), the triply differential RI cross section is shown for bare Xe colliding with various (one-electron) targets at $\tilde{E}_0 = 100$ keV as a function of θ'_k. The cross section is peaked at smaller angles than in the target frame (due to relativistic retardation effects, i.e. non-dipole transitions [37]). At the short-wavelength limit the peak intensity decreases with decreasing Z_T. However, it passes the bremsstrahlung limit and falls a factor of 2 short for $Z_T \leqslant 1$ as expected from the discussion above. On the other hand, if one moves away from the cusp (e.g. for $\omega' = 60$ keV, also shown in figure 3(a)), the bremsstrahlung limit is already reached for $Z_T = 1$ (the cross section resulting from $Z_T = 1$ is indistinguishable from the limit $Z_T = 0$ in figure 3(a)).[2] It is worthwhile noting that, in contrast to the behaviour at the SWL, the cross section maximum increases with decreasing Z_T due to the underlying Compton profile. The reason for the different behaviour of photons when emitted simultaneously with cusp electrons is the superposition of the cusp structure in the electron spectrum on the Compton-profile background [33]. As concerns the corresponding photon polarization (shown in figure 3(b)), the bremsstrahlung limit is reached for $Z_T = 1$ at all photon energies (except at the SWL for $\theta'_k \approx 0$).

---

[2] The contradictory behaviour found in figure 5 of [38] is due to a numerical error in the relativistic code. In fact, the correct RI result is indistinguishable from the Elwert–Haug theory.
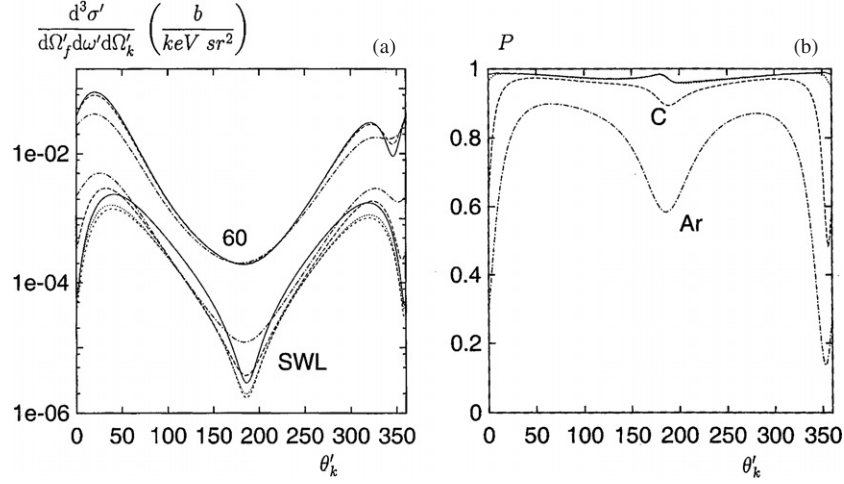
Figure 3. Projectile-frame triply differential cross section (a) and polarization (b) for K-shell RI from Xe^{54+} + T as a function of θ'_k. Chain curve, T = Ar ($Z_T = 18$); long-broken curve, C ($Z_T = 6$); dotted curve, H ($Z_T = 1$); short-broken curve, $Z_T = 0.3$ and full curve, $Z_T = 0$. The parameters are $\tilde{E}_0 = 100$ keV, $\theta'_f = 10°$, $\varphi = 0$. The upper bunch of curves is for $\omega' = 60$ keV, the lower bunch is at the SWL ($\omega' = 94.71, 99.4, 99.97, 99.984, 99.985$ keV for $Z_T = 18, 6, 1, 0.3, 0$, respectively). In (b) all curves correspond to the SWL.

4. Structure of the cross section and spin-flip transitions

In order to get a better understanding of the RI process we have to look more closely at the radiation matrix element (A.1) which is governed by the operator $\boldsymbol{I}$.

From the inspection of the explicit formulae (A.3)–(A.5) for $\boldsymbol{I}$ one expects a maximum in the differential cross section when the prefactor $|N_0|$ becomes large. One possibility is that $\tilde{\alpha}$ tends to zero, which for example is related to a cross section maximum in (e, 2e) reactions [39, 40]. However, due to the smallness of the photon momentum (in the weak-relativistic regime considered here) this is not the case for RI; in fact, the differential cross section is largest if photon and electron are emitted into the *same* half-plane [16, p 15] (see also figure 3(a)).

As a second possibility, a maximum in the differential cross section could be produced when $\tilde{\gamma} \to 0$. One has (with $\epsilon = +0$)

$$\tilde{\gamma} = \tfrac{1}{2}[q^2 - (\boldsymbol{k}' + \boldsymbol{k}'_f)^2] + \mathrm{i}\epsilon q \tag{4.1}$$

where in the bremsstrahlung limit $q^2 = \gamma^2 v^2$ is a large quantity. If one considers the coplanar geometry, $\tilde{\gamma}$ small requires $\theta'_k \approx \theta'_f$ (for $\varphi = 0$) or $\theta'_k + \theta'_f \approx 0$ (for $\varphi = 180°$). If $\theta'_k \approx \theta'_f \approx 0$ then $\tilde{\alpha}$ is small in addition.

Figure 4 shows the ω'-dependence of the pair (θ'_k, θ'_f) which leads to the maximum in the triply differential cross section $\frac{\mathrm{d}^3\sigma'}{\mathrm{d}\Omega'_f \, \mathrm{d}\omega' \, \mathrm{d}\Omega'_k}$ for an Ag^{47+} projectile colliding with various targets. It is seen that in the SWL ($\omega' \approx 300$ keV) the corresponding angles are quite large for a hydrogen target, but they decrease when ω' gets smaller and also when the target gets heavier. Note that when ω' decreases, k'_f increases (see (2.7)) such that the dependence of $\tilde{\gamma}$ on $\theta'_k + \theta'_f$ gets stronger. This produces the ω'-dependent shift to smaller angles (which is also known from bremsstrahlung investigations [16, p 124]). The reason why, particularly for loosely bound electrons, both angles are still quite large (except for the smallest values
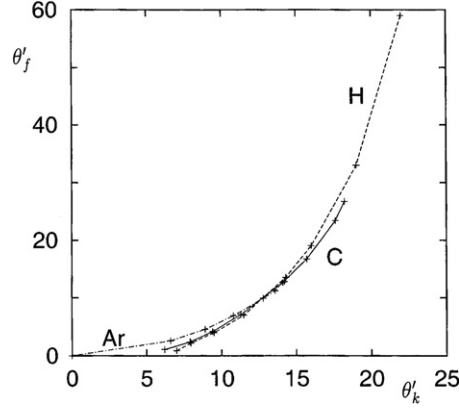
Figure 4. Pair of angles (θ'_k, θ'_f) at $\varphi = 0$ leading to the maximum of the projectile-frame triply differential K-shell RI cross section for Ag^{47+} + T and $\tilde{E}_0$=300 keV. The targets are H (— — —), C (————) and Ar (— · — · —). The crosses on each curve, starting from the left end, mark the sequence of frequencies $\omega' = 50, 100, 150, 200, 250, 270, 290$ keV and the SWL ($\omega' = 299.9, 299.2, 293$ keV, respectively, for H, C, Ar). The curves are guides to the eye.

of ω') is the strong reduction of zero-angle differential cross sections since they are basically induced by spin-flip transitions.

The influence of spin-flip transitions is most readily explained in the bremsstrahlung limit (3.9). The spin-flip contributions to the differential cross section, originating from the two pairs $(\sigma_i, \sigma_f) = (1, 2)$ and $(2, 1)$, are due to the occurrence of $\boldsymbol{\alpha}$-matrices in the transition operator $e_\lambda \boldsymbol{I}$. One has $\alpha_l \alpha_k = \begin{pmatrix} \sigma_l \sigma_k & 0 \\ 0 & \sigma_l \sigma_k \end{pmatrix} = -\alpha_k \alpha_l$ with σ_k, $k \in \{x, y, z\}$, a Pauli matrix and $\sigma_x \sigma_y = i\sigma_z$ (with cyclic permutations). If the presence of the small components in the Dirac spinors $u_q^{(\sigma)}$ is neglected, only the combinations $\alpha_x \alpha_z$ and $\alpha_y \alpha_z$ lead to spin-flip transitions.

In the particular case of collinear particle emission (when $\boldsymbol{k}'_f$ and $\boldsymbol{k}'$ are aligned with $\boldsymbol{v}$), the bremsstrahlung limit, $\boldsymbol{q} = -\gamma \boldsymbol{v}$, leads to an alignment of the momentum transfer $\boldsymbol{p}_0$ and hence of $\boldsymbol{I}_1$ with the z-axis (see (A.6)). Since the polarization directions e_λ now lie in the (x, y)-plane, the contribution of $e_\lambda \boldsymbol{I}$ proportional to I_0 and to the last term of (A.3) cause spin flip, whereas $e_\lambda \boldsymbol{I}_1 = 0$. Therefore, in the nonrelativistic (bremsstrahlung) theory the cross section for collinear particle emission is zero [29].

Let us now consider the non-collinear case and allow for arbitrary $\boldsymbol{q}$. With the choice of coplanar geometry and $\lambda = \lambda_1$ (perpendicular polarization) we have $\boldsymbol{p}_0 = (p_{0x}, q_y, p_{0z})$ and from (A.6) $\boldsymbol{I}_1 = (I_{1x}, q_y(I_{10} + I_{11}), I_{1z})$ with $I_{1x} = p_{0x}I_{10} + q_x I_{11} + k'_{fx}I_{12}$ (and the corresponding definition for the z-component I_{1z}).

Insertion into (A.3) and using $\alpha_y^2 = 1$ leads to

$$
\begin{aligned}
e_{\lambda_1} \boldsymbol{I} = \alpha_y I_0 &+ \left[\frac{cp_{0z}}{2E'_f} I_0 + \frac{icq}{2} \left(\frac{1}{E'_f} - \frac{1}{E_q} \right) I_{1z} \right] \alpha_z \alpha_y \\
&+ q_y \left[\frac{c}{2E'_f} I_0 + \frac{icq}{2} \left(\frac{1}{E'_f} + \frac{1}{E_q} \right) (I_{10} + I_{11}) \right] \\
&+ \left[\frac{c}{2E'_f} (p_{0x} I_0 + iq I_{1x}) - \frac{icq}{2E_q} I_{1x} \right] \alpha_x \alpha_y.
\end{aligned}
\tag{4.2}
$$
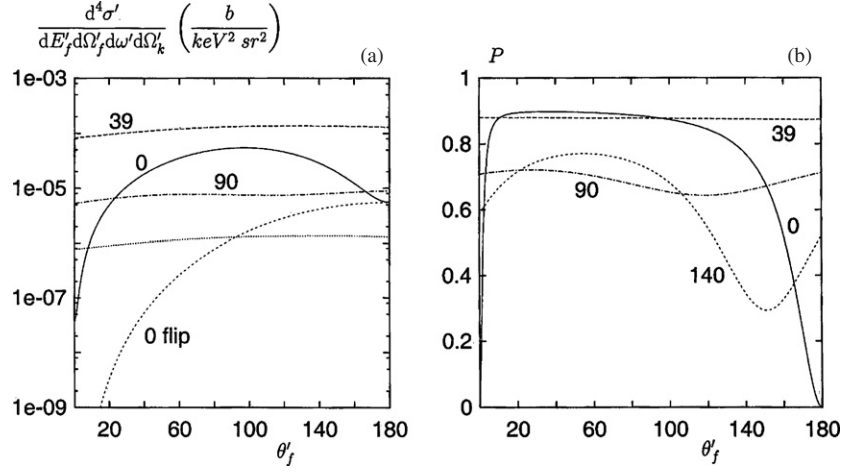
Figure 5. Projectile-frame four-fold differential RI cross section (a) and polarization (b) from Ag^{47+} + H at $\tilde{E}_0 = 300$ keV as a function of θ'_f at $\theta'_k = 0°$ (————), 39° (corresponding to $\vartheta_k = 90°$, — — —), 90°(— · — · —). The short-broken and dotted curves give, respectively, the spin-flip contributions for $\theta'_k = 0°$ and 90°. The parameters are $\varphi = 0$, $E'_{f,kin} = 10^{-3}$ keV and $\omega' = \omega'_{peak}$. In (b), the polarization for $\theta'_k = 140°$ is included (- - - -).

The terms of the first line cause spin-flip transitions whereas the remaining terms are spin conserving (if the small components are neglected).

Figure 5(a) shows the differential RI cross section from Ag^{47+} + H collisions at the SWL as a function of the electron emission angle. For $\theta'_k = 0$, the cross section is indeed purely spin flip if $\theta'_f = 180°$ whereas it is strongly reduced near $\theta'_f = 0$. Since the four-fold differential RI cross section for a hydrogen target shows a similar angular dependence as the bremsstrahlung limit [38], one may adopt the Fano *et al* [29] result that the forward radiation for $\theta'_f \approx 0$ is suppressed because of a mutual cancellation of the Feynman terms corresponding to radiation before, respectively after the electron–nucleus interaction (strictly speaking, the Born approximation of [29] is not applicable at the SWL, but similar results are also found for smaller values of ω').

At larger θ'_k, the spin-flip contribution is mostly one order of magnitude smaller than the (non-flip) contribution from the orbital currents. The general unimportance of spin-flip effects is globally true in the weak-relativistic regime considered here (see, e.g., figure 2(a)).

Figure 6(a) depicts the differential RI cross section at $\theta'_f = 10°$ as a function of the photon emission angle for different collision energies. The minima near 0 and 180° are very pronounced, and the spin-flip contribution increases with projectile velocity. This reflects the fact that the higher the γ, the more important become the small components of the Dirac spinors such that additional spin-flip transitions come into play. In contrast, a higher projectile charge does not necessarily lead to an increase of the spin-flip effects.

5. Cusp asymmetry

When studying the cusp electrons one has to keep in mind that the nonradiative electron capture to continuum (ECC) occurs simultaneously with the RI, in particular for the lower collision energies and the heavier targets. As a guideline, the velocity v_{cr} may be defined where in the cusp maximum the RI integrated over the photon degrees of freedom provides the same intensity as ECC. For $v > v_{cr}$, RI will then be dominating. Considering the continuum
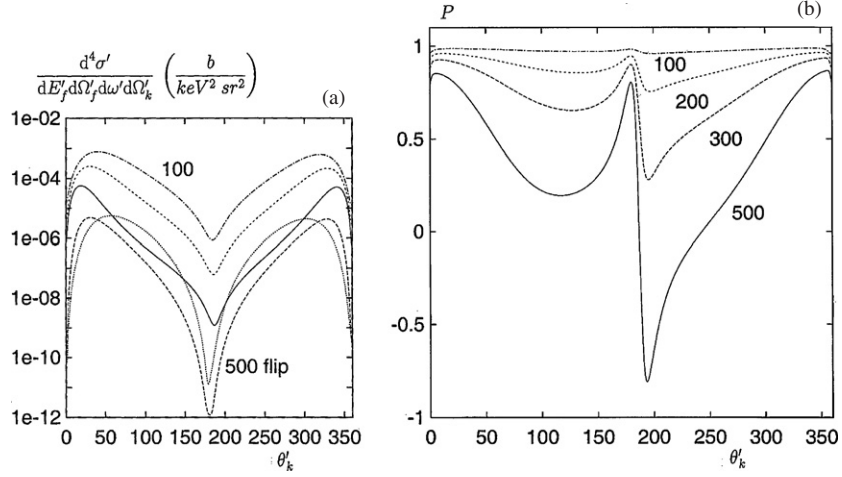
Figure 6. Projectile-frame four-fold differential RI cross section (a) and polarization (b) from Ag^{47+} + H as a function of θ'_k for $\tilde{E}_0 = 100$ keV ($- \cdot - \cdot -$), 200 keV (- - - -) and 500 keV (———) as well as the spin-flip contribution for 100 keV ($\cdots\cdots$) and 500 keV (— — —). The parameters are $E'_{f,kin} = 1.5 \times 10^{-2}$ keV, $\theta'_f = 10°$, $\varphi = 0$ and $\omega' = \omega'_{peak}$. In (b), polarization for $\tilde{E}_0 = 300$ keV is included (— — —).

capture of a target 1s electron, the dependence of v_{cr} on the target nuclear charge may be approximated by the linear formula $\gamma v_{cr} = aZ_T + b$ (with $a = 11.3$ and $b = 9$ au), which is accurate to 5% for $Z_T \leqslant 10$ and to 10% for $Z_T \leqslant 18$ within the impulse approximation (and Sommerfeld–Maue wavefunctions) for both processes. A detailed discussion of RI and ECC as competing processes is provided in [3].

As concerns the specific cusp features, we will concentrate on the cusp asymmetry. In contrast to the ECC, the RI cusp is skewed to the high-energy side [33]. This feature has just been confirmed by experiment, colliding 90 MeV amu^{-1} U^{88+} beams with nitrogen [1, 2]. Such a comparison with experiment requires the averaging of the doubly differential cross section $d^2\sigma/dE_f \, d\Omega_f$ over the detector resolution.

A more direct access to the cusp phenomena, unveiled by the detector resolution, is provided by using inverse kinematics: the bremsstrahlung process of quasifree electrons in the short-wavelength limit as viewed from the projectile reference frame. Due to the transformation rules (2.4) and (3.10) the forward electrons on the high-energy side of the cusp correspond in the projectile frame to electrons with $k'_f \approx 0$ and $\theta'_f = 180°$ whereas the electrons on the low-energy side refer to $k'_f \approx 0$ and $\theta'_f = 0$. From figure 5(a), it is clearly seen that the four-fold differential cross section at the cusp ($E'_{f,kin} \equiv E'_f - mc^2 = 10^{-3}$ keV) is higher at $\theta'_f = 180°$ than at $\theta'_f = 0$, particularly for $\theta'_k = 0$.

However, this behaviour changes with electron energy. Figure 7 displays the θ'_k-dependence of the ratio $A = d^4\sigma'(180°)/d^4\sigma'(0)$. At the cusp, this ratio is above unity for all photon emission angles, but when the electron energy E'_f is increased there is an angular region where the ratio falls below 1. The higher the E'_f the more extended this region, reflecting the fact that in the target frame the low-energy electrons are ejected with a much higher intensity than the fast electrons.

Figure 8 shows the backward-to-forward ratio at the cusp for different projectiles and different collision velocities. At the values of θ'_k corresponding to the cross section maximum (and thus giving the dominant contribution to the doubly differential cusp cross section),
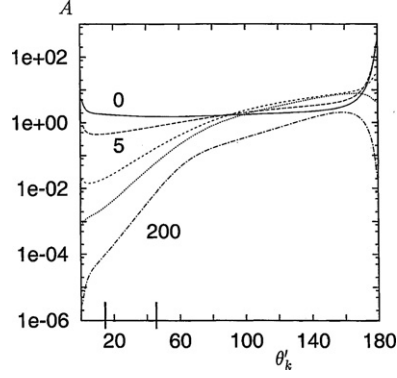
Figure 7. Asymmetry ratio A of the projectile-frame four-fold differential cross section $\mathrm{d}^4\sigma'/\mathrm{d}E'_f\,\mathrm{d}\Omega'_f\,\mathrm{d}\omega'\,\mathrm{d}\Omega'_k$ for K-shell RI from Ag^{47+} + (one-electron) C taken at $\theta'_f = 180°$ and $0°$, respectively, as a function of θ'_k. The kinetic electron energy $E'_{f,\mathrm{kin}}$ is, respectively, 10^{-3} keV (———), 5 keV (— — —), 50 keV (- - - -), 100 keV (·········) and 200 keV (— · — · —). The parameters are $\tilde{E}_0 = 300$ keV, $\varphi = 0$, $\omega' = \omega'_{\mathrm{peak}}$. The interval on the abscissa bounded by the vertical lines marks the θ'_k-region where the maximum of the four-fold differential cross sections is located (for $\theta'_f = 0°$, $180°$).
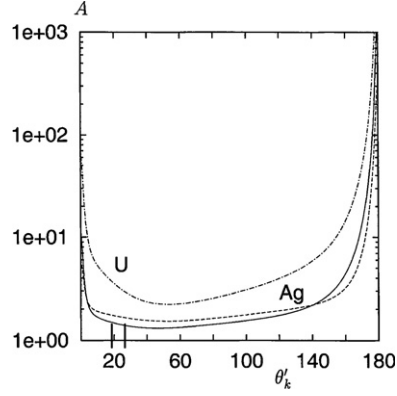
Figure 8. Asymmetry ratio A for K-shell RI from Ag^{47+} + (one-electron) C at $\tilde{E}_0 = 300$ keV (— — —) and 500 keV (———) and from U^{92+} + (one-electron) C at $\tilde{E}_0 = 500$ keV (— · — · —) as a function of θ'_k. The parameters are $E'_{f,\mathrm{kin}} = 10^{-3}$ keV, $\varphi = 0$, $\omega' = \omega'_{\mathrm{peak}}$. For the meaning of the vertical lines see the caption of figure 7.

the ratio decreases with the collision velocity and increases with projectile charge. A more systematic investigation of this feature (for doubly differential RI cusp cross sections) can be found in [3]. However, the velocity dependence of the backward-to-forward ratio changes with θ'_k. The target dependence is rather weak (except for θ'_k near 0 or $180°$ where a H target leads to a higher ratio than, e.g., a C target).

6. Photon polarization

For coplanar geometry (where $\boldsymbol{v}$, $\boldsymbol{k}'_f$ and $\boldsymbol{k}'$ lie in the (x, z)-plane) the photon is polarized in-plane in the nonrelativistic bremsstrahlung theory. Recall that this is based on the fact that,
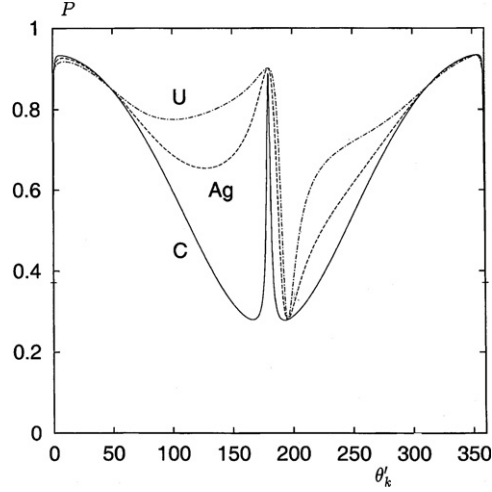
Figure 9. Polarization corresponding to the projectile-frame four-fold differential RI cross section for P + H as a function of θ'_k. The projectiles are C^{6+} (————), Ag^{47+} (— — —) and U^{92+} (—·—·—). The parameters are $\tilde{E}_0 = 300$ keV, $E'_{f,kin} = 1.5 \times 10^{-2}$ keV, $\theta'_f = 10°$, $\varphi = 0$, $\omega' = \omega'_{peak}$.

nonrelativistically, $e_\lambda I$ from (3.9) has the structure

$$e_\lambda I^{nr} = e_\lambda \left(q I_0^{nr} + I_1^{nr} \right) \tag{6.1}$$

where I_0^{nr} is a scalar function and I_1^{nr} has the form of (A.6) with I_{1k} replaced by I_{1k}^{nr}, $k = 0, 1, 2$ (and $p_0 \equiv q - k'_f$). Since $q = -v$, p_0 lies in the (x, z)-plane and so does I^{nr}, resulting in $e_{\lambda_1} I^{nr} = 0$ and hence $P = 1$. Any deviation from $P = 1$ in RI is thus based either on relativistic effects or on the binding of the electron in its initial state. From (4.2) it follows that for increasing collision velocity the spin-conserving terms in the last line increase in magnitude since they are of order v/c. For the same reason, the spin-flip terms increase but also the small components of the wavefunctions gain more importance. When, on the other hand, the initial-state momentum distribution of the electron is broadened such that q_y attains larger values, $e_{\lambda_1} I$ increases too. This causes the decrease of P with γ and for the heavier targets.

Figure 3(b) shows the Z_T-dependence of the polarization. For hydrogen, deviations from the bremsstrahlung limit occur only for near-zero degree photons. However, when the target gets heavier, P drops considerably. It thereby follows the rule, known from bremsstrahlung investigations ([8, 30] for the SWL, [31, 41] for an experimental overview), that photon angles for which the cross section shows minima provide the largest deviation of P from unity, whereas the location of the cross section maxima corresponds to the highest in-plane polarization. This is related to the fact that cross section minima arise from high momentum transfer, necessitating close collisions where both relativistic and binding effects are probed most effectively.

The projectile-charge dependence of P, again in the SWL, is given in figure 9 for the projectile reference frame and in figure 2(b) for the target reference frame. Clearly, the more dominant the in-plane polarization, the heavier the projectile. The decrease of the perpendicular polarization with increasing Z_P has been discussed and observed experimentally for bremsstrahlung from 300 keV e + C, Cu, Au (at a lower frequency, $\omega' = 160$ keV [32]).
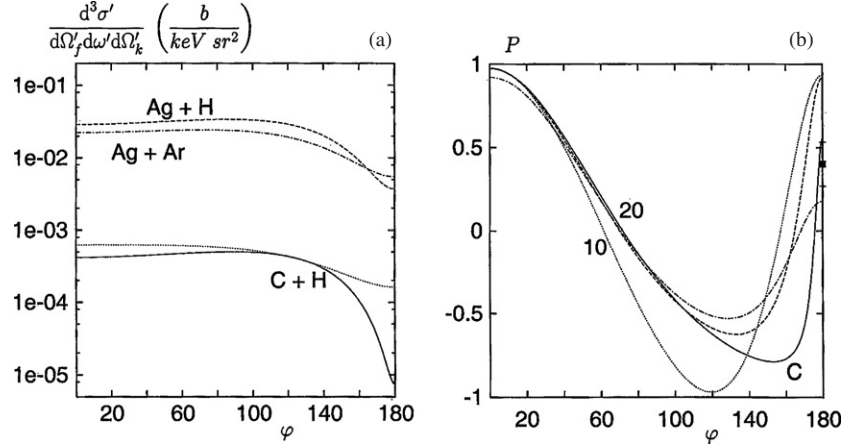
Figure 10. Projectile-frame triply differential cross section (a) and polarization (b) for K-shell RI as a function of azimuthal angle φ. Considered are $C^{6+} + H$ at $\theta'_k = 20°$ (———) and $10°(\cdots\cdots\cdots)$ as well as $Ag^{47+} + H$ (— — —) and $Ag^{47+} + Ar$ (— · — · —) at $\theta'_k = 20°$. The other parameters are $\tilde{E}_0 = 300$ keV, $\theta'_f = 20°$, $\omega' = 160$ keV. In (b), the measurement of Behnke and Nakel [31] for 300 keV e + C and $\theta'_k = 20°$ is included (●).

For collinear particle emission one has rotational symmetry leading to $e_{\lambda_1} I = e_{\lambda_2} I$ and hence $P = 0$ (see figure 5(b) for $\theta'_k = 0$, $\theta'_f \in \{0, 180°\}$, but also figure 11(b) relating to the target-frame differential cross sections for $\vartheta_f = 0$, $\vartheta_k \in \{0, 180°\}$). However, the decrease of P from near unity to 0 is confined to a very small angular region close to $0°$ and $180°$, respectively. Any slight breaking of rotational symmetry (figures 1(b) and 2(b) for $\vartheta_f = 1°$) fills the minimum and shifts it to higher ϑ_k.

The depolarization with increasing γ is shown in figure 6(b) at the SWL where v is increased from 75.13 au ($\gamma = 1.2$) to 118.25 au ($\gamma = 2$). The transformation to the target frame of reference destroys this monotonicity of decrease (see figure 1(b)) but also there the more prominent the oscillations of P, the higher the v. Note that for the heavy Ar target even $v = 26.72$ au ($\gamma = 1.02$) leads to a 15% deviation from $P = 1$.

7. Non-coplanar geometry

To our knowledge, the case where the electron is not ejected into the plane determined by v and k' has not yet been considered in the study of the polarization of bremsstrahlung photons. The variation of the azimuthal angle φ in the interval $0° < \varphi < 180°$ provides another realm of structures both of the differential cross section and of P. The most striking feature is the loss of correspondence of the cross section minima to maximum depolarization. In fact, even in the nonrelativistic bremsstrahlung limit, strong deviations of P from unity occur when φ is varied. Figure 10 shows RI for the collision of C^{6+} with H at $v = 106.4$ au ($\gamma = 1.6$) which in the inverse kinematics corresponds to 300 keV e + C, the system investigated by Behnke and Nakel [31] in their polarization study. Clearly, the triply differential cross section at the experimental choice of parameters ($\theta'_k = \theta'_f = 20°$, $\varphi = 180°$, $\omega' = 160$ keV) remains approximately constant up to $\varphi \approx 140°$. The largest depolarization is found near $\varphi = 150°$ where the cross section is only a factor of 2 below its value at $\varphi = 0$. This feature is preserved
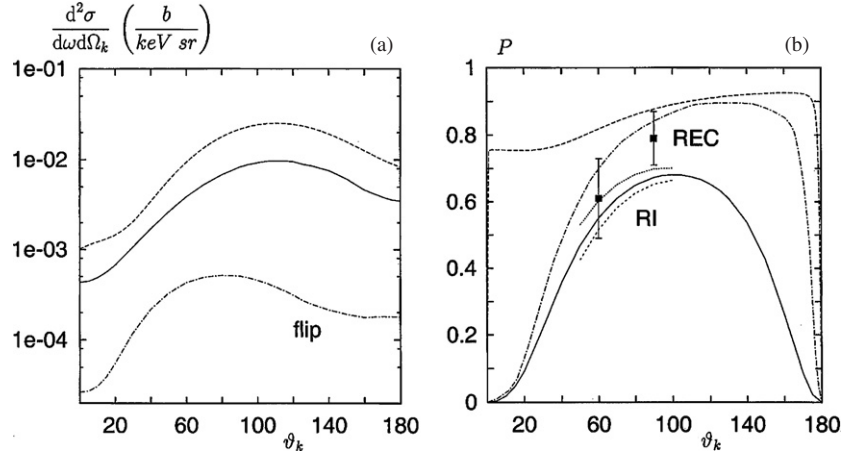
Figure 11. Doubly differential SWL cross section (a) and polarization (b) for RI from U^{92+} + H as a function of photon angle ϑ_k. Shown is the cross section (summed over λ, ———) and its spin-flip contribution ($- \cdot - \cdot -$) for $\tilde{E}_0 = 300$ keV and $\omega = \omega_{\text{peak}}(\vartheta_k)$ determined from $E_{\text{f,kin}} = \tilde{E}_0$. Also shown is the four-fold differential cross section $\mathrm{d}^4\sigma/\mathrm{d}E_f\,\mathrm{d}\Omega_f\,\mathrm{d}\omega\,\mathrm{d}\Omega_k$ (in b/keV^2 sr^2) for the same system at $\vartheta_f = 1°$, $\varphi = 0$ and $E_{\text{f,kin}} = \tilde{E}_0$ (———). In (b), the polarization corresponding to the four-fold differential cross section at $\vartheta_f = 0$, $\varphi = 0$ and $E_{\text{f,kin}} = \tilde{E}_0$ is shown instead (— — —), and the polarization resulting from the doubly differential cross section at $\tilde{E}_0 = 218$ keV ($\cdots\cdots\cdots$) and 350 keV (- - - -) is included. Comparison is made with rigorous relativistic polarization calculations for K-shell REC from 400 MeV amu^{-1} U^{92+} colliding with an electron target ($- \cdot - \cdot -$, [25]) and with experiment using a nitrogen target (■, [22]).

when projectile and target are varied. Whereas P decreases with decreasing projectile charge for nearly all values of φ, it is no longer generally true that P also decreases with Z_T.

8. Comparison with radiative electron capture

Consider the differential cross section from (2.1) integrated over the electron degrees of freedom with a photon emitted at the short-wavelength limit,

$$\frac{\mathrm{d}^2\sigma_\lambda}{\mathrm{d}\omega\,\mathrm{d}\Omega_k} = \int_{c^2}^{\infty} \mathrm{d}E_f \int \mathrm{d}\Omega_f \frac{\mathrm{d}^4\sigma_\lambda}{\mathrm{d}E_f\,\mathrm{d}\Omega_f\,\mathrm{d}\omega\,\mathrm{d}\Omega_k}, \tag{8.1}$$

and define the (linear) polarization according to (2.6). Continuity across the ionization threshold assures that (8.1) agrees with the doubly differential cross section for REC into a bound projectile state of main quantum number n (summed over the quantum numbers l, m) as $n \to \infty$. Incidentally, REC by a fast heavy projectile leads predominantly to ground-state capture, for which the relativistic (spin-flip) effects and the Z_P-dependence are expected to be stronger than for capture into the continuum states. However, since both processes, RI at the SWL and REC into the K-shell, require close collisions with the projectile since they are highly inelastic processes, some similarities are expected.

For the comparison between RI and REC (figure 11) we have chosen a collision system where pioneer measurements of the REC photon polarization have been carried out [22]. The experiment was performed for 400 MeV amu^{-1} U^{92+} on a nitrogen target. The experimental points result from photon intensities which comprise all photons in the REC peak region and thus correspond to singly differential REC cross sections obtained by integrating over the projectile Compton profile. However, when the peak frequency is selected in the doubly

differential cross section, the ϑ_k-dependence should not be much different. The target species is not important for the doubly differential RI cross section since (8.1) implies an integration over the target Compton profile. Therefore, we have compared with RI using a hydrogen target. The impact energy is varied from 400 MeV amu^{-1} (corresponding to $\tilde{E}_0 = 217.9$ keV) to 643 MeV amu^{-1} (corresponding to $\tilde{E}_0 = 350$ keV, i.e. to electrons the energy of which is increased by the U K-shell binding energy). The effect on the polarization is only minor (see figure 11(b)). We note that the ϑ_k-dependence of P is quite similar for RI and REC, except at very large angles.

The spin-flip contribution to the RI differential cross section (figure 11(a)) is, independently of ϑ_k, one order of magnitude below the spin-conserving contribution. This should be contrasted to the REC results for the singly differential K-shell capture cross section where for the forward photon emission angles (and also at 180°) the spin-flip contribution is strongly dominant [21].

In figure 11(a), we have included the result from the four-fold differential RI cross section for the same collision system at $\vartheta_f = 1°$ and $E_f = 300$ keV. The ϑ_k-dependence of the doubly and the four-fold cross section is much alike. However, the corresponding polarization (figure 2(b)) is very different. This is similar to the findings in the bremsstrahlung theory [31].

9. Conclusion

We have investigated the dependence of the differential cross section for radiative ionization on the momenta of the emitted electron and photon when both particles are observed simultaneously. The discussion is much simplified if the momentum distributions are viewed from the projectile frame of reference because there electron and photon energy approximately add up to γmc^2, without involving the emission angles.

Using the correspondence between the cusp electrons and the photons at the short-wavelength limit, we have found that the cusp asymmetry strongly depends on the photon emission angle. The asymmetry is particularly large at angles near 0° or 180°, where it even increases with collision velocity in contrast to the results obtained when the photon is not observed. If the electrons acquire a finite kinetic energy $E'_{f,kin}$, the asymmetry can get reversed at specific angles.

This decisive difference between RI cusp electrons and electrons with finite $E'_{f,kin}$ (say, $\gtrsim 5$ keV) becomes also visible in the way how the bremsstrahlung limit is reached when the target nuclear charge is decreased to zero. Whereas for 'off-cusp' electrons this limit is approached monotonically for all photon angles and is reached at $Z_T \approx 1$, the differential cross section for the cusp electrons lies a factor of 2 below the bremsstrahlung limit for $Z_T \lesssim 1$.

A related phenomenon is the excellent agreement of the (photon or electron) angular distribution for 'off-cusp' electrons when calculated, respectively, from the triply and four-fold differential cross section (where E'_f is integrated over, respectively fixed at the peak value), whereas there occur deviations for the cusp electrons. All these derivations can be traced back to the fact that on a background which is shaped by the target Compton profile there the cusp-like peak structure is superimposed.

As concerns the photon polarization we have, in the coplanar geometry, confirmed the results from investigations of the elementary bremsstrahlung process that the maximum depolarization correlates to the minima in the differential cross section. This correspondence is lost, however, in the non-coplanar geometry where large depolarization and large differential cross sections can coexist.

We have carried out a systematic study of the dependence of P on the photon energy as well as on the photon angle for fixed electron emission angle, restricting ourselves to the

coplanar geometry. When at fixed electron energy (e.g. at the cusp) the photon energy is varied across the Compton profile, there is hardly any change of P (in the region where the differential cross section has dropped by two orders of magnitude). When the photon energy moves away from the SWL (and the electron energy takes the peak value for each ω'), there is hardly any change of P either except possibly for heavier targets (where the depolarization increases when ω' is lowered). On the other hand, P varies strongly with photon angle and this feature depends in addition on the choice of reference frame. We have confirmed the findings from the elementary bremsstrahlung process that in the minima of P the depolarization decreases with the projectile charge and increases with γ. We have also found that P decreases with the target nuclear charge (for the one-electron targets considered here). But again, this behaviour may change with photon emission angle.

Finally, the photon-angle dependence of P from RI is in qualitative agreement with experiments on the elementary bremsstrahlung process and on the radiative electron capture into the projectile ground state, as expected from the similarity of these three processes. This makes us confident that the Sommerfeld–Maue wavefunctions, applied in the present work, provide at least a qualitative description of both the differential RI cross section and the associated photon polarization.

Acknowledgments

Appendix

We give the result for the radiation matrix element when Sommerfeld–Maue wavefunctions are used. For its derivation see [33].

We define $\boldsymbol{I}$ by means of

$$\boldsymbol{W}_{\mathrm{rad}}(\sigma_{\mathrm{f}}, s, \boldsymbol{q}) = \frac{1}{(2\pi)^3} e^{\pi\eta_q/2}\Gamma(1 - \mathrm{i}\eta_q)e^{\pi\eta_f/2}\Gamma(1 - \mathrm{i}\eta_f)\left(u_{k'_f}^{(\sigma_{\mathrm{f}})+}\boldsymbol{I}u_q^{(s)}\right) \tag{A.1}$$

where the 4-spinors are given by

$$u_q^{(1)} = \sqrt{\frac{E_q + c^2}{2E_q}}\begin{pmatrix} 1 \\ 0 \\ vq_z \\ vq_+ \end{pmatrix}, \qquad u_q^{(2)} = \sqrt{\frac{E_q + c^2}{2E_q}}\begin{pmatrix} 0 \\ 1 \\ vq_- \\ -vq_z \end{pmatrix} \tag{A.2}$$

with $E_q = \sqrt{q^2c^2 + c^4}$, $v = c/(E_q + c^2)$ and $q_\pm = q_x \pm \mathrm{i}q_y$. Then

$$\boldsymbol{I} = \boldsymbol{\alpha}\left[1 + \frac{c}{2E'_f}(\boldsymbol{\alpha}\boldsymbol{p}_0)\right]I_0 + \frac{\mathrm{i}cq}{2}\left[\frac{2}{E'_f}\boldsymbol{I}_1 - \boldsymbol{\alpha}\left(\frac{1}{E'_f} - \frac{1}{E_q}\right)(\boldsymbol{\alpha}\boldsymbol{I}_1)\right] \tag{A.3}$$

where $\boldsymbol{p}_0 = \boldsymbol{q} - \boldsymbol{k}' - \boldsymbol{k}'_f$ is the momentum transferred to the projectile nucleus, and

$$I_0 = N_0\left\{-\,_2F_1\left(1 - \mathrm{i}\eta_q, \mathrm{i}\eta_f, 1; \frac{\tilde{\alpha}\tilde{\delta} - \tilde{\beta}\tilde{\gamma}}{\tilde{\alpha}(\tilde{\gamma} + \tilde{\delta})}\right)[\eta_f(k'_f\tilde{\gamma} - q\tilde{\delta}) + \eta_q q(\tilde{\gamma} + \tilde{\delta})]\right.$$
$$\left. -\,_2F_1\left(2 - \mathrm{i}\eta_q, 1 + \mathrm{i}\eta_f, 2; \frac{\tilde{\alpha}\tilde{\delta} - \tilde{\beta}\tilde{\gamma}}{\tilde{\alpha}(\tilde{\gamma} + \tilde{\delta})}\right)\frac{(1 - \mathrm{i}\eta_q)\tilde{\gamma}\eta_f}{\tilde{\alpha}(\tilde{\gamma} + \tilde{\delta})}\right.$$

$$\times [q\tilde{\delta}(\tilde{\alpha} + \tilde{\beta}) - k'_f \tilde{\gamma}(\tilde{\alpha} + \tilde{\beta} + \tilde{\gamma} + \tilde{\delta})]\Big\}$$

$$N_0 = 2\pi e^{-\pi\eta_q} \tilde{\alpha}^{i\eta_q - 1} \tilde{\gamma}^{i\eta_f - i\eta_q - 1} (\tilde{\gamma} + \tilde{\delta})^{-i\eta_f - 1}. \tag{A.4}$$

$_2F_1$ is a hypergeometric function and $\tilde{\alpha} = \frac{1}{2}(p_0^2 + \epsilon^2)$, $\tilde{\beta} = k'_f p_0 - i\epsilon k'_f$, $\tilde{\gamma} = qp_0 + i\epsilon q - \tilde{\alpha}$, $\tilde{\delta} = qk'_f + qk'_f - \tilde{\beta}$ with $\epsilon = +0$. Further,

$$\begin{aligned}
I_1 = N_0 \Bigg\{ {}_2F_1 &\left(1 - i\eta_q, i\eta_f, 1, \frac{\tilde{\alpha}\tilde{\delta} - \tilde{\beta}\tilde{\gamma}}{\tilde{\alpha}(\tilde{\gamma} + \tilde{\delta})}\right) \\
&\times \left[-i\eta_f \tilde{\gamma}\left(p_0 + k'_f \frac{q}{q} + k'_f\right) + i(\eta_f - \eta_q)p_0(\tilde{\gamma} + \tilde{\delta})\right] \\
&+ {}_2F_1\left(2 - i\eta_q, 1 + i\eta_f, 2, \frac{\tilde{\alpha}\tilde{\delta} - \tilde{\beta}\tilde{\gamma}}{\tilde{\alpha}(\tilde{\gamma} + \tilde{\delta})}\right) i\eta_f(1 - i\eta_q) \frac{(\tilde{\alpha} + \tilde{\beta})\tilde{\gamma}}{\tilde{\alpha}(\tilde{\gamma} + \tilde{\delta})} \\
&\times \left[\tilde{\gamma}k'_f \frac{q}{q} + \tilde{\gamma}k'_f - \tilde{\delta}p_0\right]\Bigg\}. \tag{A.5}
\end{aligned}$$

Note that I_1 is a linear combination of the vectors p_0, q and k'_f, i.e. it can be written in the following form:

$$I_1 = p_0 I_{10} + q I_{11} + k'_f I_{12} \tag{A.6}$$

where I_{10}, I_{11} and I_{12} are the corresponding coefficients.

References

[1] Nofal M et al 2006 GSI Scientific Annual Report 2005 p 304
[2] Nofal M et al 2007 Phys. Rev. Lett. (submitted)   See endnote 1
[3] Jakubaßa-Amundsen D H 2007 Eur. Phys. J. D **41** 267
[4] Jakubaßa D H and Kleber M 1975 Z. Phys. A **273** 29
[5] Bethe H A and Heitler W 1934 Proc. R. Soc. A **146** 83
[6] Bess L 1950 Phys. Rev. **77** 550
[7] Maximon L C and Bethe H A 1952 Phys. Rev. **87** 156
[8] Elwert G and Haug E 1969 Phys. Rev. **183** 90
[9] Tseng H K and Pratt R H 1971 Phys. Rev. A **3** 100
[10] Shaffer C D, Tong X-M and Pratt R H 1996 Phys. Rev. A **53** 4158
[11] Keller S and Dreizler R M 1997 J. Phys. B: At. Mol. Opt. Phys. **30** 3257
[12] Tseng H K 2002 J. Phys. B: At. Mol. Opt. Phys. **35** 1129
[13] Lichtenberg W, Przybylski A and Scheer M 1975 Phys. Rev. A **11** 480
[14] Aehlig A, Metzger L and Scheer M 1977 Z. Phys. A **281** 205
[15] Nakel W 1994 Phys. Rep. **243** 317
[16] Haug E and Nakel W 2004 The Elementary Process of Bremsstrahlung (World Scientific Lecture Notes in Physics vol 73) (Singapore: World Scientific)
[17] Lucas M W, Steckelmacher W, Macek J and Potter J E 1980 J. Phys. B: At. Mol. Phys. **13** 4833
[18] Eichler J and Stöhlker Th 2007 Phys. Rep. **439** 1
[19] Ichihara A, Shirai T and Eichler J 1994 Phys. Rev. A **49** 1875
[20] Stöhlker Th et al 1997 Phys. Rev. Lett. **79** 3270
[21] Stöhlker Th et al 1999 Phys. Rev. Lett. **82** 3232
[22] Tashenov S et al 2006 Phys. Rev. Lett. **97** 223202
[23] Tseng H K and Pratt R H 1973 Phys. Rev. A **7** 1502
[24] Pratt R H, Levee R D, Pexton R L and Aron W 1964 Phys. Rev. **134** A916
[25] Surzhykov A, Fritzsche S, Stöhlker Th and Tachenov S 2003 Phys. Rev. A **68** 022710
[26] Eichler J and Ichihara A 2002 Phys. Rev. A **65** 052716
[27] Gluckstern R L and Hull M H Jr 1953 Phys. Rev. **90** 1030
[28] Gluckstern R L, Hull M H Jr and Breit G 1953 Phys. Rev. **90** 1026

[29] Fano U, McVoy K W and Albers J R 1959 *Phys. Rev.* **116** 1159
[30] Haug E 1969 *Phys. Rev.* **188** 63
[31] Behnke H-H and Nakel W 1978 *Phys. Rev.* A **17** 1679
[32] Bleier W and Nakel W 1984 *Phys. Rev.* A **30** 607
[33] Jakubaßa-Amundsen D H 2003 *J. Phys. B: At. Mol. Opt. Phys.* **36** 1971
[34] Kirkpatrik P and Wiedmann L 1945 *Phys. Rev.* **67** 321
[35] Bjorken D and Drell S D 1964 *Relativistic Quantum Mechanics* (Mannheim: BI)
[36] Davidović D M, Moiseiwitsch B L and Norrington P H 1978 *J. Phys. B: At. Mol. Phys.* **11** 847
[37] Spindler E, Betz H-D and Bell F 1979 *Phys. Rev. Lett.* **42** 832
[38] Jakubaßa-Amundsen D H 2006 *Radiat. Phys. Chem.* **75** 1319
[39] McCarthy I E and Weigold E 1976 *Phys. Rep.* C **27** 275
[40] Jakubaßa-Amundsen D H 1995 *J. Phys. B: At. Mol. Opt. Phys.* **28** 259
[41] Nakel W 2006 *Radiat. Phys. Chem.* **75** 1164

Endnotes

(1) Author: Please update reference [2].
(2) Author: Please check the figure 10 caption symbol (●) here. Do you mean (■)?

Reference linking to the original articles

References with a volume and page number in blue have a clickable link to the original article created from data deposited by its publisher at CrossRef. Any anomalously unlinked references should be checked for accuracy. Pale purple is used for links to e-prints at arXiv.